Simulation of Heat Transport in Graphene Nanoribbons Using the Ab-Initio Scattering Operator

Proceedings of the ASME 2014 International Mechanical Engineering Congress and Exposition
IMECE2014
November 14-20, 2014, Montreal, Quebec, Canada

IMECE2014-36473

SIMULATION OF HEAT TRANSPORT IN GRAPHENE NANORIBBONS USING THE AB-INITIO SCATTERING OPERATOR

Colin D. Landon
Department of Mechanical Engineering
Massachusetts Institute of Technology
Cambridge, MA 02139
Email: clandon@mit.edu

Nicolas G. Hadjiconstantinou
Department of Mechanical Engineering
Massachusetts Institute of Technology
Cambridge, MA 02139
Email: ngh@mit.edu

ABSTRACT

We present a deviational Monte Carlo method for simulating phonon transport in graphene using the ab initio 3-phonon scattering operator. This operator replaces the commonly used relaxation-time approximation, which is known to neglect, among other things, coupling between out of equilibrium states that are particularly important in graphene. Phonon dispersion relations and transition rates are obtained from density functional theory calculations. The proposed method provides, for the first time, means for obtaining solutions of the Boltzmann transport equation with ab initio scattering for time- and spatially-dependent problems. The deviational formulation ensures that simulations are computationally feasible for arbitrarily small temperature differences; within this formulation, the ab initio scattering operator is treated using an efficient stochastic algorithm which, in the limit of large number of states, outperforms the more traditional deterministic methods used in solutions of the homogeneous Boltzmann equation. We use the proposed method to study heat transport in graphene ribbons.

INTRODUCTION

Transport in graphene-based devices with length scales in the 10nm-10μm range is expected to be an area of considerable interest for some time, both because of the difficulty associated with manufacturing large area graphene sheets, but also due to the interest associated with the development of small scale electronic devices. Due to the relatively long phonon mean free path, Fourier-based descriptions cannot be used [1] to describe graphene devices with these length scales [2]. In response to these challenges, in this paper, we present a new Monte Carlo method for solving the phonon Boltzmann transport equation (BTE) with ab initio scattering for modeling phonon transport in two-dimensional materials in general and graphene in particular.

Methods for solving the BTE with ab initio scattering have been limited to calculations of the bulk thermal conductivity of materials using iterative formulations [1, 3]. More recently, a variational method for solving this problem has also been developed [4]. Both of these approaches obtain solutions of the BTE assuming spatially homogeneous, steady state conditions and by assuming that the effect of boundaries can be modeled by introducing an additional (homogenous) scattering rate. In contrast, the method presented here does not require any of the above assumptions, since it is able to solve the BTE for arbitrary spatial and temporal variations.

The technique proposed here is based on the low variance deviational simulation Monte Carlo (LVDSMC) [5–9], an efficient stochastic method for obtaining solutions of the BTE. In this paper, we present and discuss the algorithmic developments necessary for treating the ab initio collision operator and its discrete representation in reciprocal space. We also present some results from simulations of phonon transport in graphene ribbons. Our results are used to quantify the error associated with augmenting the homogeneous Boltzmann equation with an additional scattering rate to model the effect of transverse boundaries in infinitely long graphene ribbons. Two-dimensional simulation results for transport in nanoribbons of finite width and length are also presented and discussed.

THEORETICAL MODEL

In this work we consider the Boltzmann transport equation

$$\frac{\partial n}{\partial t} + \mathbf{v}(\mathbf{q},s)\cdot\nabla_{\mathbf{x}} n = \left[\frac{\partial n}{\partial t}\right]_{\text{scatt}} \tag{1}$$

where $n(\mathbf{x},\mathbf{q},s,t)$ is the single-phonon distribution function, $\mathbf{x}$ denotes spatial position, $\mathbf{q}$ the reciprocal space wavevector, s phonon polarization and t time. This description is typically referred to as semiclassical because it treats phonons as particles by neglecting coherence and interference effects; this can be justified by noting that at the lengthscales of interest here ($L > 10$nm), these effects are expected to be small [8]. Ab initio information is retained by use of quantum-mechanically-derived dispersion relations and, as elaborated below, a scattering model derived from density-functional theory.

The present work takes a step towards improving the fidelity of semiclassical Monte Carlo simulations by replacing the ubiquitous single mode relaxation approximation with the ab initio three-phonon scattering operator in two dimensions [10]

$$\begin{aligned}\left[\frac{\partial n_\lambda}{\partial t}\right]_{\text{3-ph}} = {} & \frac{A_{\text{uc}}}{2\pi\hbar^2}\sum_{s',s''}\int \mathrm{d}^2\mathbf{q}'\,|\tilde{\mathscr{V}}_3(-\lambda,-\lambda',\lambda'')|^2\delta_{\text{I}} \\ & \times\big((n_\lambda+1)(n_{\lambda'}+1)n_{\lambda''} - n_\lambda n_{\lambda'}(n_{\lambda''}+1)\big) \\ & + \frac{A_{\text{uc}}}{4\pi\hbar^2}\sum_{s',s''}\int \mathrm{d}^2\mathbf{q}'\,|\tilde{\mathscr{V}}_3(-\lambda,\lambda',\lambda'')|^2\delta_{\text{II}} \\ & \times\big((n_\lambda+1)n_{\lambda'}n_{\lambda''} - n_\lambda(n_{\lambda'}+1)(n_{\lambda''}+1)\big)\end{aligned} \tag{2}$$

where A_{uc} is the area of the real space unit cell, λ is used to denote the combined dependence of n on $\mathbf{q}$ and s, $\delta_{\text{I}} = \delta(-\omega_\lambda - \omega_{\lambda'} + \omega_{\lambda''})$ imposes energy conservation for type-I processes, $\delta_{\text{II}} = \delta(-\omega_\lambda + \omega_{\lambda'} + \omega_{\lambda''})$ imposes energy conservation for type-II processes and ω_λ denotes the frequency of phonon mode λ. Note that in this expression, in the interest of simpicity, the spatial and time dependence of the distribution function are not shown explicitly. Also, $\tilde{\mathscr{V}}_3(-\lambda,-\lambda',\lambda'')$ denotes the interaction strength of the corresponding three-phonon process; in the present work, it is obtained from density functional theory calculations: force constants for graphene were provided by K. Esfarjani and S. Lee and were obtained using the methodology described in Ref. [11].

Due to the small temperature gradients of interest here, we assume that the deviation from equilibrium is small ($n^{\text{d}}_\lambda = n_\lambda - n^0_\lambda \ll n^0_\lambda$), to obtain the linearized form of the collision operator

$$\begin{aligned}\left[\frac{\partial n^{\text{d}}_\lambda}{\partial t}\right]_{\text{scatt}} = {} & \frac{A_{\text{uc}}}{2\pi\hbar^2}\sum_{s',s''}\int \mathrm{d}^2\mathbf{q}'\,|\tilde{\mathscr{V}}_3(-\lambda,-\lambda',\lambda'')|^2\delta_{\text{I}} \times \\ & \big((n^0_{\lambda''}-n^0_\lambda)n^{\text{d}}_{\lambda'} + (n^0_\lambda + n^0_{\lambda'}+1)n^{\text{d}}_{\lambda''} + (n^0_{\lambda''}-n^0_{\lambda'})n^{\text{d}}_\lambda\big) \\ & + \frac{A_{\text{uc}}}{4\pi\hbar^2}\sum_{s',s''}\int \mathrm{d}^2\mathbf{q}'\,|\tilde{\mathscr{V}}_3(-\lambda,\lambda',\lambda'')|^2\delta_{\text{II}} \times \\ & \big((n^0_{\lambda''}-n^0_\lambda)n^{\text{d}}_{\lambda'} + (n^0_{\lambda'}-n^0_\lambda)n^{\text{d}}_{\lambda''} - (n^0_{\lambda''}+n^0_{\lambda'}+1)n^{\text{d}}_\lambda\big)\end{aligned} \tag{3}$$

Here, $n^0_\lambda = n^0(\omega_\lambda;T_0)$ is an appropriately chosen Bose-Einstein (equilibrium) distribution; the control temperature T_0 may be chosen as a function of space as a means of improving variance reduction or imposing temperature gradients on the material [6,7,9].

SIMULATION METHOD

As shown previously [5,6,9], deviational methods are significantly more efficient than traditional Monte Carlo methods because they simulate only the deviation from equilibrium. This results in drastically reduced statistical uncertainty, but also the ability to automatically and adaptively concentrate the computational effort in regions where kinetic effects are important, which is of great importance in the simulation of multiscale phenomena [6,9,12].

The developments discussed below are specific to the linearized operator (3). However, we note that the assumption of small deviation from equilibrium is not required for the LVDSMC methodology which is valid for arbitrary deviations from equilibrium (e.g see Ref. [13]); simulations of the nonlinear operator (2) will be considered in the future.

Currently, the collision operator (3) can only be evaluated numerically by discretizing reciprocal space; in this work we use the parallepiped unit cell shown in Figure 1. We then use a two dimensional implementation of the linear tetrahedra method [14,15] to perform the integration over $\mathbf{q}'$ in (3) and write the linearized scattering operator [2,4] in the form

$$\left[\frac{\partial n^{\text{d}}_i}{\partial t}\right]_{\text{scatt}} = \sum_{j=1}^{N_{\text{states}}} A_{ij} n^{\text{d}}_j \tag{4}$$

where N_{states} is the number of discrete reciprocal states and i indexes the discrete state with wavevector $\mathbf{q}_i$ and polarization s_i.

The transition matrix is given by

$$A_{lm} = \frac{A_{\mathrm{uc}}}{2\pi\hbar^2}\frac{1}{n_m^0(n_m^0+1)} \Big(\sum_{ijk}[N_{\mathrm{I}}(i,j,k)W_{\mathrm{I}}(i,j,k)\left(-\delta_{im}\delta_{ml}-\delta_{il}\delta_{jm}+\delta_{il}\delta_{km}\right) + N_{\mathrm{II}}(i,j,k)W_{\mathrm{II}}(i,j,k)\left(-\delta_{im}\delta_{ml}+\delta_{il}\delta_{jm}+\delta_{il}\delta_{km}\right)]\Big) \quad (5)$$

where $W_{\mathrm{I}}(i,j,k)$, and $W_{\mathrm{II}}(i,j,k)$ are the coefficients resulting from the linear interpolation [2], $N_{\mathrm{I}}(i,j,k) = n_i^0 n_j^0(n_k^0+1)$ and $N_{\mathrm{II}}(i,j,k) = \frac{1}{2}(n_i^0+1)n_j^0 n_k^0$.

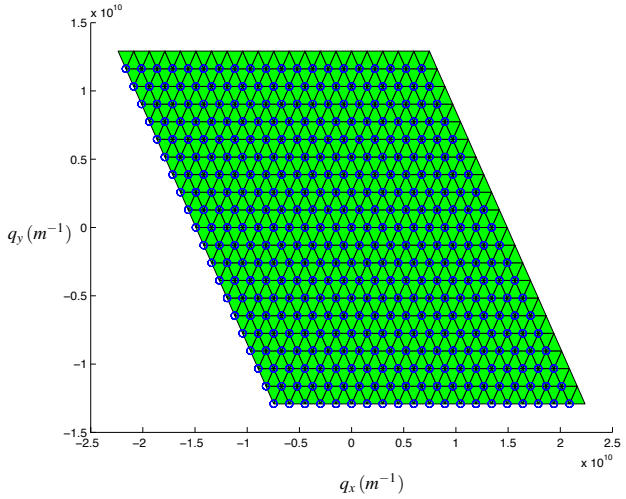

FIGURE 1. Parallelepiped unit cell used to discretize reciprocal space. Only the circled vertices are included in the computational mesh—the vertices on the right and top boundaries are equivalent to those on the left and bottom boundaries, respectively, via periodicity. Here a $N_{\mathrm{states}} = 2397$ discretization is shown—6 branches with 400 states in each branch, with the Γ point for the three acoustic branches removed.

Following recent work [6], we pursue an energy conserving algorithm by simulating the energy distribution

$$f_i = \frac{2}{A_{\mathrm{uc}}N_{\mathrm{tri}}\delta}\hbar\omega_i n_i \quad (6)$$

where N_{tri} is the number of triangles in the reciprocal space discretization and δ is the thickness of graphene. Formally, the distribution function is approximated by a collection of N_{parts} particles by writing

$$f_i^{\mathrm{d}} = \sum_{j=1}^{N_{\mathrm{parts}}} E_{\mathrm{eff}}\sigma_j\delta_{\lambda_j,\lambda_i}\delta(\mathbf{x}-\mathbf{x}_j) \quad (7)$$

where E_{eff} is the effective energy that each computational particle represents and σ_j is the sign (± 1) of particle j. Equation (7) highlights the fact that this work uses a discrete representation of the reciprocal space required by the scattering model, but a continuous representation of physical space. The dynamics of these "deviational" particles follow [6, 7, 9] from

$$\frac{\partial f_i^{\mathrm{d}}}{\partial t} + \mathbf{v}_i\cdot\nabla_{\mathbf{x}}f_i^{\mathrm{d}} + \mathbf{v}_i\cdot\nabla_{\mathbf{x}}f_i^0 = \sum_j B_{ij}f_j^{\mathrm{d}} \quad (8)$$

where $B_{ij} = (\omega_i/\omega_j)A_{ij}$ and $f_i^0 = (2/A_{\mathrm{uc}}N_{\mathrm{tri}}\delta)\hbar\omega n_i^0$.

As is typical in direct Monte Carlo simulation methods, integration of this equation utilizes four main algorithmic ingredients: initialization, sampling, advection and scattering. The advection and scattering substeps form the core of the integration algorithm which proceeds using a timestep of duration Δt. Implementation details are discussed by Péraud and Hadjiconstantinou for three-dimensional phonon simulations [6] and Landon and Hadjiconstantinou [8] for two dimensional materials. Here, we briefly describe the algorithm with particular emphasis on the changes required for simulating two-dimensional materials using a formulation which is discrete in reciprocal space and features the ab initio scattering operator.

Initialization

Initialization requires sampling particles from a prescribed distribution function (initial condition). For steady problems, it is convenient to initialize a simulation from the reference equilibrium so that $f_i^{\mathrm{d}} = 0$. In that case, no particles need to be generated. In the more general case where a simulation needs to be initialized from an arbitrary (non-equilibrium) distribution, $f_i(\mathbf{x}, t=0)$, this leads to

$$f_i^{\mathrm{d,init}}(\mathbf{x}, t=0) = f_i(\mathbf{x}, t=0) - f_i^0. \quad (9)$$

Particles from this distribution can be generated by acceptance-rejection [2]; any physical space dependence is handled by discretizing physical space in cells. More sophisticated methods for sampling a distribution function in the context of stochastic particle simulation of the Boltzmann equation have also been developed [16] and may provide additional computational gains.

Sampling

In order to sample properties, the continuous spatial domain is divided into cells of volume $V_{\text{cell}} = A_{\text{cell}}\delta$; spatial variation in properties can be calculated in a cell-averaged sense. For example, the energy density in cell m of volume V_{cell} is given by

$$u_m = \frac{\sum_{\{j|\mathbf{x}_j \in \text{cell } m\}} E_{\text{eff}}\sigma_j}{V_{\text{cell}}} + u_{\text{eq}}(T_0) \tag{10}$$

where $u_{\text{eq}}(T_0)$ is the (equilibrium) energy density at the reference (control) temperature T_0. The heat flux is given by

$$\mathbf{J}_{E,m} = \frac{1}{V_{\text{cell}}} \sum_{\{j|\mathbf{x}_j \in \text{cell } m\}} E_{\text{eff}}\sigma_j \mathbf{v}_j \tag{11}$$

We have found that due to numerical errors in calculating the third order force constants and due to finite discretization of the reciprocal space, $\mathbf{B}$ does not conserve energy and momentum exactly. This creates numerical problems for our strictly (energy) conserving scheme. In this work, we used a Lagrange multiplier optimization scheme [2] to construct an additive correction to matrix $\mathbf{B}$ such that the latter satisfies energy conservation

$$\sum_i \left[\frac{\partial f_i^{\text{d}}}{\partial t}\right]_{\text{scatt}} = 0 = \sum_{ij} B_{ij} f_j^{\text{d}} = \sum_j \Big(\underbrace{\sum_i B_{ij}}_{=0}\Big) f_j^{\text{d}} \tag{12}$$

and momentum conservation

$$\sum_i \mathbf{q}_i \left[\frac{\partial n_i^{\text{d}}}{\partial t}\right]_{\text{scatt}} = 0 = \sum_{ij} \frac{\mathbf{q}_i}{\omega_i} B_{ij}^{\text{N}} f_j^{\text{d}} = \sum_j \Big(\underbrace{\sum_i \frac{\mathbf{q}_i}{\omega_i} B_{ij}^{\text{N}}}_{=0}\Big) f_j^{\text{d}} \tag{13}$$

where $\mathbf{B}^{\text{N}}$ denotes the part of the $\mathbf{B}$ matrix that contains the normal scattering processes.

Advection

The advection sub step simulates the left hand side of (8), which can be separated into two parts. The first part,

$$\frac{\partial f_i^{\text{d}}}{\partial t} + \mathbf{v}_i \cdot \nabla_{\mathbf{x}} f_i^{\text{d}} = 0, \tag{14}$$

describes ballistic motion of particles which is implemented as $\mathbf{x}_j(t+\Delta t) = \mathbf{x}_j(t) + \mathbf{v}_j(t)\Delta t$. Note that particles move ballistically until the end of the time step or the time they encounter a boundary. Prescribed temperature boundaries are described below as an example of boundary condition treatment.

The second part of the advection sub step results from the final term on the left hand side of (8), namely

$$\mathbf{v}_i \cdot \frac{\partial f^{\text{eq}}(\omega_i;T))}{\partial T} \nabla_{\mathbf{x}} T_0(\mathbf{x}), \tag{15}$$

which is nonzero if the control temperature is chosen to be a function of space. As dicussed in a number of previous publications [6, 9] and in [2] for two-dimensional materials, this can be treated by volumetrically generating additional particles and can be useful for improving variance reduction, or introducing a temperature gradient without explicitly simulating the physical dimension in which the gradient exists.

Boundaries at prescribed temperature The net heat flux across a prescribed temperature boundary with inward normal (pointing into the material) $\hat{\mathbf{n}}_{\text{wall}}$ is given by

$$J_{E,\text{wall}} = \sum_{\{i|\mathbf{v}_i\cdot\hat{\mathbf{n}}_{\text{wall}}>0\}} \mathbf{v}_i \cdot \hat{\mathbf{n}}_{\text{wall}} f_i^{\text{wall}} + \sum_{\{i|\mathbf{v}_i\cdot\hat{\mathbf{n}}_{\text{wall}}<0\}} \mathbf{v}_i \cdot \hat{\mathbf{n}}_{\text{wall}} f_i, \tag{16}$$

where f_i^{wall} is calculated from the Bose-Einstein distribution at the wall temperature. Utilizing the reciprocal space symmetry, this can be rewritten in the form

$$J_{E,\text{wall}} = \sum_{\{i|\mathbf{v}_i\cdot\hat{\mathbf{n}}_{\text{wall}}>0\}} \mathbf{v}_i \cdot \hat{\mathbf{n}}_{\text{wall}} \left(f_i^{\text{wall}} - f_i^0\right) + \sum_{\{i|\mathbf{v}_i\cdot\hat{\mathbf{n}}_{\text{wall}}<0\}} \mathbf{v}_i \cdot \hat{\mathbf{n}}_{\text{wall}} f_i^{\text{d}}. \tag{17}$$

This can be efficiently implemented in two steps. First, particles within the simulation that encounter the boundary (proportionally to $|\mathbf{v}_i \cdot \hat{\mathbf{n}}_{\text{wall}}| f_i^{\text{d}}$) are discarded. Second, particles representing

$$J_{\text{E,wall,in}} = \sum_{\{i|\mathbf{v}_i\cdot\hat{\mathbf{n}}_{\text{wall}}>0\}} \mathbf{v}_i \cdot \hat{\mathbf{n}}_{\text{wall}} \left(f^{\text{wall}} - f_i^0\right) \tag{18}$$

are generated. More details on generating samples from the appropriate distribution, including the total number of particles that must be generated per timestep can be found in [2].

A special case of this boundary condition that is particularly easy to implement follows when the wall temperature is chosen to be the reference equilibrium temperature T_0. In this case, the particles encountering the wall are removed and no additional particles need to be generated.

Scattering

The scattering step seeks to update the particle distribution following the action of the scattering operator which can be written in the form

$$f_i^{\mathrm{d}}(t+\Delta t) = \sum_j P_{ij}(\Delta t) f_j^{\mathrm{d}}(t) \tag{19}$$

where $\mathbf{P}$ is the generator matrix given by

$$\mathbf{P}(\Delta t) = e^{\mathbf{B}\Delta t} = \sum_{k=0}^{\infty} \frac{\Delta t^k}{k!} \mathbf{B}^k.$$

Despite its similarity to a Markov chain formulation, such formulations are not applicable here for two reasons: first, f_i^{d} can take positive or negative values (since it represents a deviational quantity); second, the elements of the propagator, P_{ij}, can also be negative (a consequence of having negative off diagonal elements in $\mathbf{B}$ due to three phonon coupling). In order to prescribe particle update rules consistent with (19), we rewrite it as

$$f_i^{\mathrm{d}}(t+\Delta t) = \sum_j \frac{P_{ij}(\Delta t)}{\mathscr{P}_j} \left(\sum_{n=0}^{\infty} \left(2\frac{\mathscr{P}_j^-}{\mathscr{P}_j} \right)^n \right) f_j^{\mathrm{d}}(t), \tag{20}$$

where $\mathscr{P}_j^-$ is the sum of the absolute values of the negative elements in column j of $\mathbf{P}$, and $\mathscr{P}_j = \sum_{k=1}^{N_{\mathrm{states}}} |P_{kj}|$. Equation (20) can be implemented as follows: given a particle in state i with sign σ,

1. Transition the particle from state i to the state p where $\mathscr{P}_i = \sum_{j=1}^{N_{\mathrm{states}}} |P_{ji}|$,

$$\sum_{j=1}^{p-1} |P_{ji}| \leq \mathscr{R}\mathscr{P}_i < \sum_{j=1}^{p} |P_{ji}|,$$

   and $\mathscr{R}$ is a uniformly distributed random number in $[0,1)$.
2. Assign a new sign to the particle $\sigma' = \mathrm{sgn}(P_{pi}\sigma)$.
3. If $\sigma' \neq \sigma$, generate 2 more particles at the state i, (including the same sign) and process each by going to 1

This scattering-step scheme has the convenient feature of exactly conserving energy while introducing no timestep error. Moreover, using a binary search algorithm, the cost of the collision substep per timestep can be estimated to be of $O(N_{\mathrm{parts}}\log(N_{\mathrm{states}}))$ operations; assuming (see [2] for justification) that $N_{\mathrm{parts}} \sim N_{\mathrm{states}}$, this yields a cost of $O(N_{\mathrm{states}}\log(N_{\mathrm{states}}))$, which is superior to the $O(N_{\mathrm{states}}^2)$ operations expected of a deterministic algorithm. On the other hand, the generation of additional particles is in general undesirable, because, if untreated, can cause the simulation to become unstable. In the present work, stability is achieved by canceling positive and negative particles in the same reciprocal space state and the same spatial cell. Because cancellation within the same spatial cell allows cancellation of particles at a distance, it introduces a discretization error and requires that the spatial cells be small (typically compared to the mean free path).

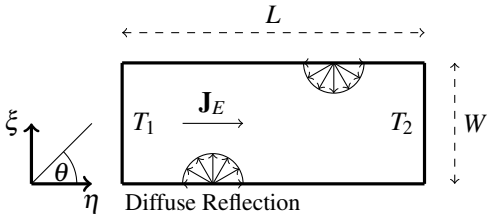

FIGURE 2. Schematic of a rectangular graphene ribbon with diffuse boundaries.

Computational results

In this section we discuss simulation results for heat transport in graphene ribbons of the geometry shown in Fig. 2 and with diffusely reflecting transverse boundaries. All results pertain to a reference temperature of 300K and have been obtained using $N_{\mathrm{states}} = 5397$. Numerical experiments show that the normalized heat flux at $Kn_W \approx 1$ changes by less than 3% when the discretization is increased from $N_{\mathrm{states}} = 5397$ to $N_{\mathrm{states}} = 14997$.

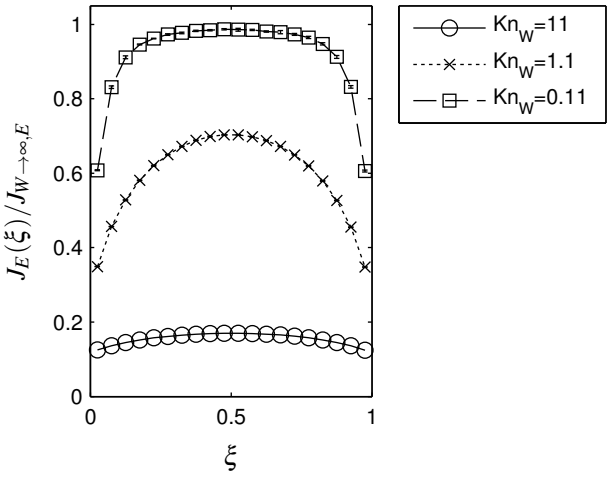

FIGURE 3. Heat flux profile across graphene ribbons of various widths calculated using LVDSMC simulations.

We first consider infinitely long ribbons of width W. Heat transport occurs due to a temperature gradient along the ribbon axis, created by taking the control temperature to vary linearly in this direction [6, 7, 9]. Figure 3 shows the heat flux profiles obtained from our simulations for various values of the Knudsen number $Kn_W = \Lambda/W$. Here, the mean free path, Λ, is defined as

$$\Lambda = \frac{\sum_i^{N_{\text{states}}} v_i \tau_i n_i^0}{\sum_i^{N_{\text{states}}} n_i^0} \tag{21}$$

where $v_i = ||\mathbf{v}_i||$, and $\tau_i = B_{ii}^{-1}$. In the figure, the (cell-averaged) heat flux in the axial direction is normalized by the value expected for an infinitely wide ribbon, denoted $J_{W\to\infty,E}$.

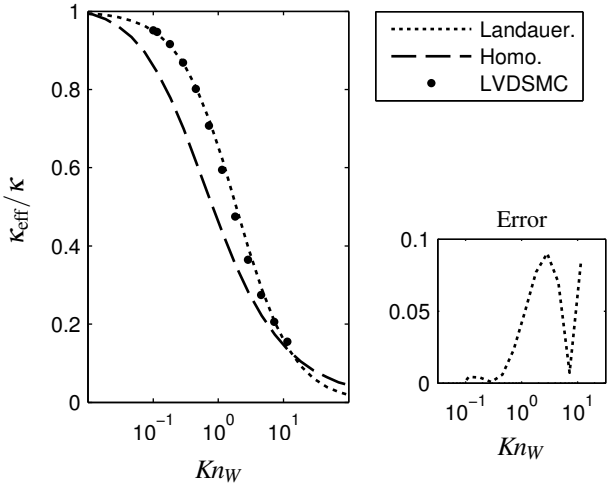

FIGURE 4. Effective thermal conductivity for an infinitely long ribbon. Comparison between LVDSMC simulations, solution of the homogeneous BTE using an augmented scattering rate to approximate boundary effects and a Landauer-like approximation. Error denotes the relative discrepancy between the Landauer and LVDSMC results.

Figure 4 shows the variation of the effective thermal conductivity of the ribbon, $\kappa_{\text{eff}} = (\kappa/J_{\to\infty,E})\int_0^1 J_E \mathrm{d}\xi$, as a function of Kn_W; here, κ denotes the bulk thermal conductivity. This figure compares MC simulation results with those obtained using the iterative solution of the homogeneous Boltzmann equation [1] in which the transverse boundaries are accounted for by augmenting phonon self-scattering with an additional scattering rate; for a rectangular ribbon this additional rate can be approximated as $2v_i|\sin(\theta_i)|/W$, where θ_i is the angle between the phonon wavevector and the ribbon longitudinal axis [18]. The figure shows that the homogeneous approximation introduces an error on the order of 30% near $Kn_W = 1$.

Figure 4 also shows that the reduction in effective thermal conductivity due to the presence of transverse boundaries can be approximately captured using a Landauer-like approach [19–22] $\kappa_{\text{eff}} = \kappa/(1+\beta_W Kn_W)$ with $\beta_W \approx 0.53$. This very simple, phenomenological model seems to capture the data well—within 10% error in the transition regime, $0.1 < Kn < 10$, which compares favorably with the homogeneous scattering rate approach.

Figure 5 shows two-dimensional simulation results for finite width and length ribbons. Transverse boundaries are again modeled as diffuse adiabatic, while boundaries in the axial (ξ) direction have prescribed temperatures. As before, heat transport takes place along the ξ direction, but this time it is due to the temperature gradient set up by the different temperatures ($T_1 \neq T_2$ in Figure 2) of the two boundaries in the ξ direction. As can be seen from the figure, the effective thermal conductivity decreases both when the ribbon length and width decrease, but it is more sensitive to the ribbon length.

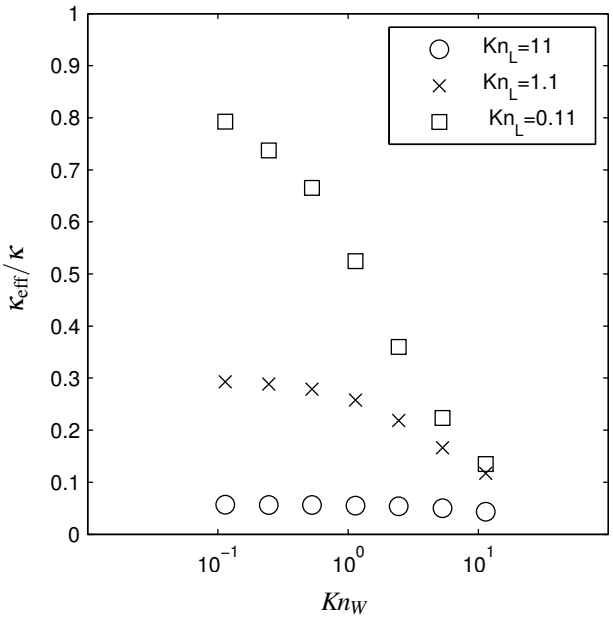

FIGURE 5. Effective thermal conductivity for ribbons of finite width and length as a function of the Knudsen numbers $Kn_L = \Lambda/L$ and Kn_W.

FINAL REMARKS

We have developed a Monte Carlo method for solving the Boltzmann equation featuring the ab initio scattering operator using transition rates from density functional theory calculations. Although more expensive than LVDMSC simulations

based on the relaxation-time approximation, the proposed formulation is sufficiently efficient to make essentially noise-free, two-dimensional simulations of graphene nanoribbons throughout the transition regime possible using modest computational resources. Despite this, the proposed methodology is still in its infancy and considerable improvements in efficiency are possible via the development, for example, of higher order discretizations in space and time as well as, perhaps, methods which treat particles independently and require no time discretization, such as the one recently developed for the relaxation-time approximation [7]. We also hope this work spurs the development of techniques for calculating force constants which lead to scattering rates with better conservation properties.

Future simulations will focus on the analysis of setups and geometries more akin to those used in experiments measuring the thermal conductivity of graphene nanoribbons.

ACKNOWLEDGMENT

The authors gratefully acknowledge financial support by the National Science Foundation Graduate Research Fellowship Program, the National Defense Science and Engineering Graduate Fellowship, and the MIT-Singapore Alliance. We are also grateful to Jean-Philippe Péraud and Sangyeop Lee for their helpful insights.

REFERENCES

[1] Mingo, N., Stewart, D., Broido, D., Lindsay, L., and Li, W., 2014. "Ab initio thermal transport". In *Length-Scale Dependent Phonon Interactions*, S. L. Shindé and G. P. Srivastava, eds., Vol. 128 of *Topics in Applied Physics*. Springer New York, pp. 137–173.

[2] Landon, C. D., 2014. "A deviational Monte Carlo formulation of ab initio phonon transport and its application to the study of kinetic effects in graphene ribbons". PhD thesis, Massachusetts Institute of Technology, Cambridge, MA.

[3] Omini, M., and Sparavigna, A., 1995. "An iterative approach to the phonon Boltzmann equation in the theory of thermal conductivity". *Physica B,* ***212***, pp. 101–112.

[4] Fugallo, G., Lazzeri, M., Paulatto, L., and Mauri, F., 2013. "Ab initio variational approach for evaluating lattice thermal conductivity". *Phys. Rev. B,* ***88***, 045430.

[5] Homolle, T., 2007. "Efficient particle methods for solving the Boltzmann equation". Master's thesis, Massachusetts Institute of Technology.

[6] Péraud, J.-P. M., and Hadjiconstantinou, N. G., 2011. "Efficient simulation of multidimensional phonon transport using energy-based variance-reduced Monte Carlo formulations". *Phys. Rev. B,* ***84***, 205331.

[7] Péraud, J.-P. M., and Hadjiconstantinou, N. G., 2012. "An alternative approach to efficient simulation of micro/nanoscale phonon transport". *Appl. Phys. Lett.,* ***101***, 153114.

[8] Landon, C. D., and Hadjiconstantinou, N. G., 2012. "Low-variance Monte Carlo simulation of thermal transport in graphene". *International Mechanical Engineering Congress and Exposition*, paper number IMECE2012-87957.

[9] Péraud, J.-P. M., Landon, C. D., and Hadjiconstantinou, N. G., 2014. "Monte Carlo methods for solving the Boltzmann transport equation". *Annu. Rev. Heat Trans.,* ***17***.

[10] Singh, D., Murthy, J. Y., and Fisher, T. S., 2011. "Spectral phonon conduction and dominant scattering pathways in graphene". *J. Appl. Phys.,* ***110***, 094312.

[11] Esfarjani, K., Chen, G., and Stokes, H. T., 2011. "Heat transport in silicon from first-principles calculations". *Phys. Rev. B,* ***84***, 085204.

[12] Radtke, G. A., Péraud, J.-P. M., and Hadjiconstantinou, N. G., 2013. "On efficient simulations of multiscale kinetic transport". *Phil. Trans. R. Soc. A.,* ***371***, 2012182.

[13] Hadjiconstantinou, N. G., Radtke, G. A., and Baker, L. L., 2010. "On variance-reduced simulations of the Boltzmann transport equation for small-scale heat transfer applications". *J. Heat Transfer,* ***132***, 112401.

[14] Kurganskii, S. I., Dubrovskii, O. I., and Domashevskaya, E. P., 1985. "Integration over the two-dimensional Brillouin zone". *Phys. Stat. Sol. B,* ***129***, pp. 293–299.

[15] Gilat, G., and Raubenheimer, L. J., 1966. "Accurate numerical method for calculating frequency-distribution functions in solids". *Phys. Rev.,* ***144***, pp. 390–395.

[16] Radtke, G. A., 2011. "Efficient simulation of molecular gas transport for micro- and nanoscale applications". PhD thesis, Massachusetts Institute of Technology, Cambridge, MA.

[17] Bird, G. A., 1994. *Molecular Gas Dynamics and the Direct Simulation of Gas Flows*. Clarendon Press.

[18] McGaughey, A. J. H., Landry, E. S., Sellan, D. P., and Amon, C. H., 2011. "Size dependent model for thin film and nanowire thermal conductivity". *Appl. Phys. Lett.,* ***99***, 131904.

[19] Landauer, R., 1987. "Electrical transport in open and closed systems". *Z. Phys B Condensed Matter,* ***68***, pp. 217–228.

[20] Pop, E., Varshney, V., and Roy, A. K., 2012. "Thermal properties of graphene: Fundamentals and applications". *MRS Bulletin,* ***37***, pp. 1273–1281.

[21] Prasher, R., 2008. "Thermal boundary resistance and thermal conductivity of multiwalled carbon nanotubes". *Phys. Rev. B,* ***77***, 075424.

[22] Jeong, C., Datta, S., and Lundstrom, M., 2011. "Full dispersion versus Debye model evaluation of lattice thermal conductivity with a Landauer approach". *J. Appl. Phys.,* ***109***, 073718.